Curtis K. Stimpson[1]
Mem. ASME
Department of Mechanical and
Nuclear Engineering,
The Pennsylvania State University,
3127 Research Drive,
State College, PA 16801
e-mail: curtis.stimpson@psu.edu

Jacob C. Snyder
Mem. ASME
Department of Mechanical and
Nuclear Engineering,
The Pennsylvania State University,
3127 Research Drive,
State College, PA 16801
e-mail: jacob.snyder@psu.edu

Karen A. Thole
Mem. ASME
Department of Mechanical and
Nuclear Engineering,
The Pennsylvania State University,
136 Reber Building,
University Park, PA 16802
e-mail: kthole@psu.edu

Dominic Mongillo
Pratt & Whitney,
400 Main Street,
East Hartford, CT 06118
e-mail: dominic.mongillo@pw.utc.com

Effectiveness Measurements of Additively Manufactured Film Cooling Holes

As additive manufacturing (AM) technologies utilizing metal powders continue to mature, the usage of AM parts in gas turbine engines will increase. Current metal AM technologies produce parts with substantial surface roughness that can only be removed from external surfaces and internal surfaces that are accessible for smoothing. Difficulties arise in making smooth the surfaces of small internal channels, which means the augmentation of pressure loss and heat transfer due to roughness must be accounted for in the design. As gas turbine manufacturers have only recently adopted metal AM technologies, much remains to be examined before the full impacts of applying AM to turbine parts are understood. Although discrete film cooling holes have been extensively studied for decades, this objective of this study was to understand how the roughness of film cooling holes made using AM can affect the overall cooling effectiveness. Coupons made from a high temperature nickel alloy with engine-scale film holes were tested in a rig designed to simulate engine relevant conditions. Two different hole sizes and two different build directions were examined at various blowing ratios. Results showed that the effectiveness is dependent on the build direction and the relative size of the hole. It was also discovered that commercially available AM processes could not reliably produce small holes with predictable behavior. [DOI: 10.1115/1.4038182]

Introduction

Additive manufacturing (AM) is receiving increasing recognition as a valuable method for producing some gas turbine components. AM provides increased design flexibility, short turnaround time for single component production, and possible economic advantages. As gas turbine designers find innovative and creative ways to design parts with the AM process in mind, AM may become the preferred manufacturing method for many gas turbine components.

For the benefits of the AM technology to be properly leveraged by the gas turbine industry that already has extensive experience in conventional manufacturing methods, creative exploration within the design space offered by AM must be fostered. However, designers must also understand the design constraints and functional implications of AM processes to generate useful designs. The current body of literature has a dearth of information necessary for designers to understand what implications their design and use of AM will have on the performance of a gas turbine component. The motivation of this study is to aid designers in understanding the implications of and constraints when using AM.

Previous research done by the current authors has aided in identifying constraints and implications related to the surface roughness on parts made with laser powder bed fusion (L-PBF), a common type of metal AM [1]. It has been shown that the roughness on L-PBF parts is significantly larger than with conventional manufacturing methods. The same causes of roughness also lead to challenges maintaining tolerances for geometries where negative features (e.g., flow channels) are not much larger than the roughness features themselves [1]. Additionally, orientation of the part relative to the build direction was seen to have direct impacts on the tolerances and roughness levels.

The authors have also previously investigated flow through small internal channels that might be used for internal cooling of turbine hardware [2–4]. As many components employ film cooling in addition to internal cooling to manage temperatures, the next step in trying to understand impacts of AM on turbine cooling designs is assessing the impact AM has on film cooling performance. Film cooling provides essential cooling to high heat load parts in the turbine engine; it is expected that AM will impact the performance of film cooling due to changes in feature tolerances and surface roughness. The uniqueness of this study was to examine the effects roughness and building tolerances have on the performance of film cooling holes built with L-PBF.

Review of Literature

Because the use of AM is still emerging in the gas turbine industry, relatively few publications have addressed applications of AM to gas turbines. Within that limited body of literature, most papers focus on characterizing the manufacturing process and the resulting material properties; only a few of them focus on the effects AM has on heat transfer performance of gas turbine parts. However, patents describing inventions with AM film cooling [5–8] and a paper written by Schurb et al. [9] clearly show that gas turbine engine manufacturers are exploring the use of AM for actively cooled turbine hardware.

Within the open literature, two papers were identified that present the thermal performance of film cooling holes made with

[1]Corresponding author.

Contributed by the International Gas Turbine Institute (IGTI) of ASME for publication in the JOURNAL OF TURBOMACHINERY. Manuscript received September 14, 2017; final manuscript received October 3, 2017; published online October 31, 2017. Editor: Kenneth Hall.

metal AM. Vinton et al. [10] studied the film effectiveness of an array of cylindrical holes made at engine scale with L-PBF. They observed decreased effectiveness for the entire array with AM holes compared to an array of smooth holes. They attributed the reduction to the roughness inside the holes but did not characterize the geometry of the holes or the roughness to compare it to their results. Jackowski et al. [11] performed similar experiments on an array of film cooling holes made with L-PBF. They studied six different hole geometries at engine relevant scales taking advantage of the additional design freedom AM allows to produce hole geometries that cannot be easily made with other manufacturing methods.

Several researchers have exploited the cost, manufacturing time, and design flexibility benefits of AM to perform experiments that likely could not have been realized with traditional manufacturing methods. Aghasi et al. [12] evaluated the use of fused deposition modeling, stereolithography, and photopolymer material jetting to quickly evaluate adiabatic effectiveness of novel film cooling hole designs. Kirollos and Povey [13] validated the use of L-PBF to produce prototypes of turbine vanes for thermal performance evaluation. This approach to product development allows for several iterations in the same amount of time it takes to produce a single prototype with conventional casting methods. Krawciw et al. [14] used L-PBF to create a panel with arrays of various shaped film cooling holes. They measured adiabatic effectiveness to evaluate performance of the array of film cooling holes. Although they used L-PBF, the film cooling holes were significantly larger than holes one might find in real engine hardware suggesting that the roughness is not as influential on their results as one might observe in an engine component made with AM.

A few investigators have examined the impact of in-hole roughness on film cooling effectiveness. Schroeder and Thole [15] performed detailed experiments with artificially roughened, shaped film holes and reported flow field, thermal field, and adiabatic effectiveness results. They showed that roughness has a significant impact on the thermal performance of film cooling holes. In particular, they found that the film cooling effectiveness was lower for holes with large relative roughness ($R_a/D \approx 0.018$). Schroeder [16] looked at the effect of spiraled grooves in a film cooling hole on its thermal performance. They found enhanced performance because of the spiral grooves as compared to axial or compound angled cylindrical holes. This was attributed to the secondary flows generated by the swirling, which altered the typical flow patterns exhibited within and near the exit of cylindrical holes.

As the roughness of AM is random in nature and its size relative to the film cooling hole diameter is very large, none of the work currently found in public literature is directly useful for predicting the thermal performance of an individual row of shaped, AM film cooling holes. This study uniquely evaluated the thermal performance of a single row of shaped film cooling holes made with AM. As this information has not been published before, this paper generates initial design guidelines that will aid gas turbine designers as they utilize the emerging and constantly evolving technologies of AM.

Study Approach

To achieve the objective of this study, several test coupons were made with L-PBF using an alloy commonly used in high temperature turbine components. In order to capture the effects that the internal roughness might have on the film cooling performance, it was essential to produce coupons with film cooling holes comparable in size to those found in operational turbine components. An experimental rig was built to hold these coupons and provide both internal and external crossflows. The approach described by Albert et al. [17] was taken in this study, whereby the dimensionless parameters of Biot number, Bi, and external to internal heat transfer coefficient ratio, h_∞/h_i, were matched to those found in engines, which implies that the results of this study can be directly applied to engines. Average Bi and h_∞/h_i for a modern engine were calculated using values reported by Bunker [18]. This section describes the test coupons, the experimental setup, and the data analysis methods.

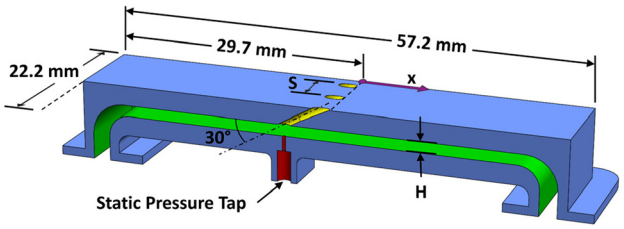

Fig. 1 Test coupon features and dimensions

Description of Test Coupons. A set of test coupons was designed to simulate hardware one might find in a gas turbine engine. An image of one of the coupons is shown in Fig. 1. The coupons have an internal channel of height H that allows coolant to flow in a co-flow configuration with that of the mainstream. Halfway along the channel, a row of film cooling holes eject coolant from the coupon through laidback fan-shaped cooling holes spaced at a specified pitch, S. The cooling hole shape selected for this study was a baseline shape proposed by Schroeder and Thole [19], which had expansion angles of 7 deg in both the forward and lateral directions and was inclined relative to the surface by 30 deg. The holes in these test coupons have the same relative dimensions for the metering length and diffuser length as did those defined in Ref. [19]. This meant that the wall thickness, t, of each coupon was dictated by the hole diameter D, meter length, and diffuser length specifications. Two different hole diameters were investigated in this study: 1× holes comparable in size to the smallest holes used in turbine components, and 2× holes that were twice that scale. The overall coupon dimensions stayed the same, but t, S, and H were adjusted to maintain the correct nondimensional parameters, hole shape, and H/D ratio. The coupons also have three static pressure ports just below the row of film holes; these were built into the coupons during the L-PBF process. The pressure taps enabled an accurate measurement of the pressure drop across the film holes.

All coupons were fabricated on a L-PBF machine during a single build using a nickel-chromium-iron-molybdenum based powdered alloy [20] with a composition matching that of Hastelloy® X. Material-specific machine parameters recommended by the L-PBF machine manufacturer were used to build the coupons [21]. Some coupon geometries were duplicated and built in a different orientation relative to the build direction. The first orientation was selected to align the axis of the film hole metering

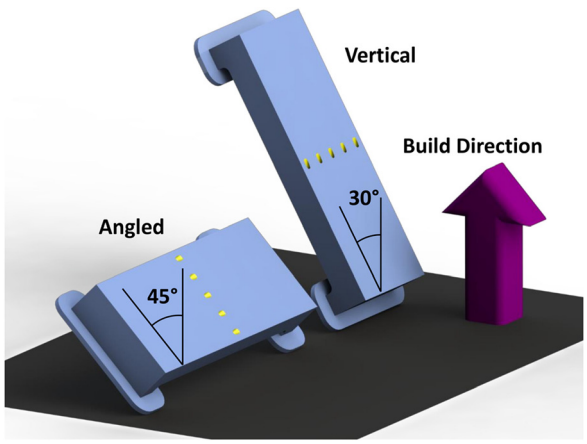

Fig. 2 Coupon orientation during build showing vertical build direction and angled build direction

section parallel with the build direction (i.e., vertical) as illustrated in Fig. 2. Previous work by the authors suggested that this would give the least amount of in-hole roughness [2]. The other selected build direction aligned the top surface of the coupon at a 45 deg angle from the build direction (i.e., angled) as shown in Fig. 2. The resulting hole was built at a 69 deg angle from the build direction (i.e., 21 deg above horizontal).

Cooling holes are rarely all aligned in the same direction on gas turbine airfoils. This means fabricating turbine components with L-PBF will result in holes with varying build orientations. The build direction will have a significant impact on the net hole shape and the in-hole roughness. This is the reason for investigating cooling performance at two different build directions. Because there are infinite build direction possibilities, ease and reliability of coupon fabrication was a key factor in selecting the orientation of the angled coupon. This build direction simplified support structure design, removal from the build plate, and support removal. Previous work by the authors suggests that this orientation would result in greater surface roughness and poorer dimensional tolerance than the vertical build orientation [2].

After fabrication, excess powder was removed, and the parts were stress relieved before removal from the plate to minimize warping. Supports were removed, and the external surfaces were ground flat and smooth. All internal surfaces of the coupon were left unaltered. External roughness features are relatively simple to remove with conventional methods, but roughness features on small internal channels, like the ones in these coupons, cannot be removed with commercial processes currently available [3]. Installing pressure tubes, painting the surface with black paint, and sanding the paint smooth were the final steps in preparing the coupon for testing. Paint was not applied in the hole to avoid reducing the hole size or roughness magnitude; the absence of paint in the holes was confirmed by inspection with a light microscope.

Eight coupons were investigated in this study. Dimensions of each coupon are given in Table 1. The coupon name listed in the first column of Table 1 provides an abbreviated description of each coupon. The first two characters in the name describe the scale of the film holes: "1×" for the small holes, and "2×" for holes that are twice that scale. The next two characters describe the build direction: "A" for the coupons with the film hole built at an angle and "V" for the coupons with the film holes built in the vertical direction. The next two characters describe the channel height scale: "1H" for the low H/D ratio and "2H" for the H/D ratio twice that of the 1H. The final group of characters denote the manufacturing method used to produce the holes: "AM" for coupons with film cooling holes that were built in the L-PBF machine, "electrical discharge machining (EDM)" for cooling holes that were drilled with plunge EDM into coupons built with L-PBF, and "BL" for baseline coupons that were also built with L-PBF and contained no film cooling holes. All coupons with film holes had a pitch to diameter ratio of $S/D = 6$. Only one coupon (1x-45-2H-EDM) had holes that were drilled with plunge EDM.

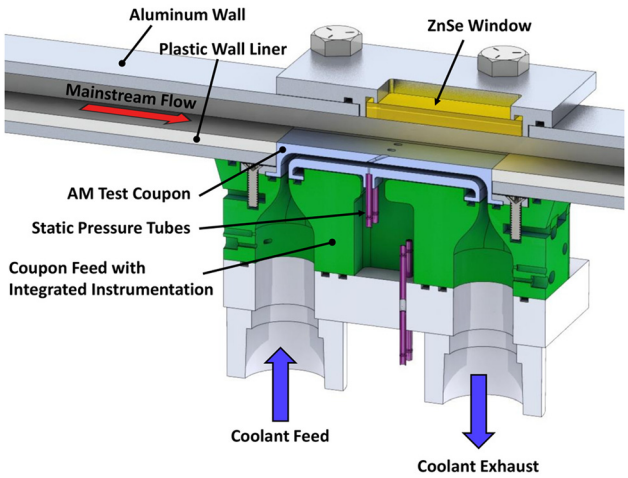

Fig. 3 Test rig developed for this study

Holes were drilled with EDM in one coupon for purposes of comparing a commonly used hole fabrication technique to film holes made with L-PBF. Although the holes were made using EDM, the coupon itself was made using AM so that the roughness elements from the AM build were present in the coolant supply channel.

Experimental Setup. The experimental rig, shown in Fig. 3, was developed to facilitate cooling effectiveness measurements of the test coupons. It was designed to supply coolant to the coupon channel while simultaneously providing a crossflow over the external surface in the same direction as the coolant flow. The intention of using this configuration was to simulate components in turbines that are exposed to high heat loads and are actively cooled to reduce part temperature. Rig dimensions were chosen to represent engine conditions by matching parameters such as h_∞/h_i and film hole blowing ratio, M, during experiments. Note that the coolant supply can be adjusted to be co-flowing or counter-flowing, but this particular study only used the co-flowing coolant configuration.

The external crossflow was supplied with dry, compressed air at a nominal temperature, and pressure of 25 °C and 4 bar. The flow rate of the air was measured with a turbine flow meter. A pressure regulator installed upstream of the rig and a throttling valve installed downstream of the test section allowed control of the supply pressure and mainstream flow rate. The mainstream air traveled through an aluminum rectangular channel that was nominally 25.4 mm in width and 9.5 mm in height. The bottom and sidewalls were lined with polyamide strips to minimize reflections of irradiation and heat conduction from the coupon to the highly conductive aluminum channel walls. The channel was sufficiently long upstream to achieve hydrodynamically developed flow before passing over the coupon.

Table 1 Test coupon dimension specifications and measurements

Coupon name	Symbol	Design, $D_{h,i}$ (mm)	Design, t (mm)	Number of holes	Design, D (mm)	Design, A_{min} (mm^2)	Build direction	Measured, $D_{h,i}$ (mm)	Measured, t (mm)	Measured, $A_{min,avg}$ (mm^2)
1x-A-2H-EDM	✕	2.45	1.14	9	0.381	0.114	Angled	1.78	1.18	0.107
1x-A-2H-AM	✱	2.45	1.14	9	0.381	0.114	Angled	1.76	1.20	0.0377
1x-V-1H-AM	○	1.26	1.14	9	0.381	0.114	Vertical	0.93	1.17	0.0760
1x-A-1H-AM	◇	1.26	1.14	9	0.381	0.114	Angled	0.72	1.20	0.0278
2x-V-1H-AM	●	2.45	2.29	5	0.762	0.456	Vertical	2.10	2.30	0.405
2x-A-1H-AM	◆	2.45	2.29	5	0.762	0.456	Angled	1.89	2.32	0.281
1x-V-1H-BL	○	1.26	1.14	—	—	—	Vertical	0.91	1.18	—
1x-A-2H-BL	✕	2.45	1.14	—	—	—	Angled	1.68	1.23	—
2x-V-1H-BL	●	2.45	2.29	—	—	—	Vertical	1.80	2.31	—
2x-A-1H-BL	◆	2.45	2.29	—	—	—	Angled	2.07	2.26	—

To match a relevant coolant jet-to-mainstream density ratio (DR), the coolant used in these experiments was cooled gaseous carbon dioxide (CO_2) fed from a liquid dewar. The flow rate of coolant was measured using a laminar flow meter placed downstream of the test section. This measurement accounted for the flow exiting the coupon but not the flow exiting the film cooling holes. Because the flow rate through the film holes is a small fraction of the total amount of coolant flowing through the coupon channel, the flow through the film holes was not directly measured during heat transfer experiments. Attempting to calculate the flow through the film holes as the difference between the coolant feed and the coolant exhaust flow rates would result in unacceptably large uncertainty.

Flow rates through the film holes were measured in a separate experiment where the coolant exhaust was sealed off and there was no external cross-flow. The flow rate through the holes was measured with a mass flow meter appropriately sized for low flow rates. The pressure ratio, $PR = P_c/P_\infty$, was simultaneously measured across the film holes at various mass flow rates. Putting the mass flow rate in terms of a nondimensional flow parameter, $FP = \dot{m}_f\ (RT_c)^{0.5}/P_cA_c$, compensated for variations in temperature, pressure, and gas type between the flow experiments and the heat transfer experiments. The PR versus FP data was used to determine the flow rate through the film holes during the heat transfer experiments by measuring only the PR.

Additive manufacturing was exploited in the designing of the experimental rig to enhance instrumentation. The part, labeled as the Coupon Feed with Integrated Instrumentation in Fig. 3, was made with stereolithography. This component features a smooth contraction at the coupon inlet to provide a uniform velocity inlet to the coupon. Several ports for thermocouples and pressure taps before and after the contraction were built directly into the part to closely monitor flow conditions.

A crucial component to the rig was the zinc selenide (ZnSe) window placed above the coupon. Because the mainstream channel operated at high pressure, optical access was necessarily obtained with a window for infrared (IR) thermography measurements. ZnSe was selected as it has a nearly constant transmissivity of 0.7 over the entire infrared spectrum. The ZnSe window was mounted in an aluminum plate that was bolted to a stainless steel base. Between these plates and the aluminum channel were rubber seals that isolated the mainstream flow, the coolant flow, and the atmosphere from each other. An IR camera was positioned above the ZnSe window at an angle that allowed it to see the surface of the coupon and avoid seeing its own reflection. The selection of parameters relating to the IR measurements (e.g., emissivity and transmissivity) was validated through calibration to ensure accurate surface temperature measurements.

Five key parameters characterize the flow and heat transfer of the system. The four independent parameters are DR, Bi, h_∞/h_i, and M; the dependent parameter is overall effectiveness, ϕ. DR and Bi were held constant for the experiment; the nominal values of these three parameters are seen in Table 2 along with Mach numbers of the mainstream and coolant channels. DR was held constant during experiments by supplying CO_2 to the coupon at a constant temperature and air to the mainstream channel at a constant temperature. Bi was also held constant for all experiments. Since the wall thickness of the 1× coupons was different than the 2× coupons, h_∞ was necessarily adjusted by changing the mainstream flow rate to maintain a constant Bi.

Table 2 Operating conditions

Variable	Nominal value
Bi	0.1
h_∞/h_i	~1.0
Ma_∞	0.3
Ma_i	<0.1
DR	1.7

Finally, h_∞/h_i was maintained constant for each size scale. Because h_i could not be measured with sufficient accuracy to reliably match h_∞/h_i between the 1× and 2× coupons, the Reynolds number of the coolant channel, Re_i, downstream of the film cooling holes was maintained constant instead. As a result, h_i of the 1× coupons is expected to be slightly larger because they have a larger $R_a/D_{h,i}$ than the 2× coupons. The resulting difference in h_∞/h_i between 1× and 2× coupons is within the experimental uncertainty.

The final independent variable, M, was varied between 0.5 and 4. In defining M, the maximum velocity in the channel (i.e., the centerline velocity), U_∞, is used instead of mass-averaged velocity, V. U_∞ was calculated assuming a 1/7th power velocity profile, which results in a ratio of $V/U_\infty = 0.817$ as given in Ref. [22]. This approach was selected to be consistent with definitions of M found in literature. Keeping the aforementioned three constant parameters unchanged isolated the impact of M, relative hole size, and build direction on the overall cooling effectiveness.

To calculate operating parameters, such as Bi and h_∞/h_i, the external heat transfer coefficient on the coupon surface, h_∞, and the internal channel heat transfer coefficient, h_i, of each coupon were first determined. The external heat transfer coefficient was calculated using a formulation for thermally developing flow between two parallel flat plates with one side heated at a constant heat flux. This solution was obtained from Ref. [22] and is expressed in Eq. (1) in terms of Nu_x. The subscript x on Nu signifies the Nusselt number varies with distance, x, along the heated section. The series solution constants G_n and λ_n for a constant heat rate boundary condition are tabulated in Ref. [22]. The dimensionless length scale, x^*, is defined as $(x/D_h)/(RePr)$ where x is again the streamwise distance from the beginning of the heated section, D_h is the hydraulic diameter of the channel, and Pr is the Prandtl number. Thermally developing flow between two flat plates with one wall heated was selected because it is the best representation of the actual flow in the region near the center of the coupon.

$$Nu_x = \frac{\sum_{n=0}^{\infty} G_n \exp\left(-\lambda_n^2 x^*\right)}{2\sum_{n=0}^{\infty}\left(G_n/\lambda_n^2\right)\exp\left(-\lambda_n^2 x^*\right)} \tag{1}$$

The heat transfer coefficient of the coupon internal channel, h_i, was found using the Nu correlation presented by Stimpson et al. [4] for flow through small, rough channels made with L-PBF. The friction factor of each coupon without film holes was measured using flow rate and pressure drop data. The resulting friction factor was then used in the Nu correlation given in Ref. [4].

Once spatially resolved temperature data were collected, it was put in the nondimensional form shown in Eq. (2), which is known as the overall cooling effectiveness, ϕ

$$\phi = \frac{T_\infty - T_s}{T_\infty - T_c} \tag{2}$$

Measurement Uncertainty. Absolute uncertainty was calculated for key parameters (ϕ, Bi, DR, M, h_∞/h_i). The uncertainty in DR is a mere ±2% because it only relies on the uncertainty in temperature measurements of the coolant and mainstream flows. The ratio h_∞/h_i has a much larger uncertainty because it relies on the accuracy of the correlations used to predict the heat transfer coefficients. The uncertainty in h_∞/h_i is approximated to be 15–30% for all conditions tested and was largely driven by the uncertainty in h_i. The Biot number was certain within ±28%. The uncertainty in h_∞ and t was driving contributors to this uncertainty. The uncertainty in M was ±18% for the 1× coupons and ±11% for the 2× coupons. The driving contributor was the

accuracy of the measurement of A_{min}. Finally, uncertainty in the overall effectiveness measurement was ±7% for high blowing ratios and ±9% for low blowing ratios. The dominant factor in this was the uncertainty in the surface temperature measurement with the IR camera.

A series of experiments were carried out to determine the repeatability of the measurements. Multiple coupons were tested on different days, having uninstalled and reinstalled the coupons. The results showed a repeatability error of ±2% in the effectiveness measurements. As will be shown, the difference in ϕ between different experiments in nearly all cases is less than the absolute uncertainty. However, because the repeatability error is low, different test conditions can be compared on a relative basis with good confidence.

Characterization of Coupon Geometry

As was shown in the authors' previous work, the internal geometry of parts made with L-PBF can deviate significantly from the part specification [2,3]. Thus, it was necessary to measure the coupons' dimensions for an accurate calculation of Re_i, M, and Bi. An industrial computed tomography (CT) scanner was used to generate a three-dimensional reconstruction of each coupon and obtain detailed part dimensions. This reconstruction had a resolution (i.e., voxel size) of 35 μm, which is the minimum resolvable feature size. However, the reconstruction software's advanced surface determination algorithm is capable of deciphering the surface with precision as good as 3–4 μm [23]. This suggests that the dimensions obtained with the CT scanner are an accurate measurement of the average surface location even though it cannot resolve all the small-scale roughness features.

After the interior surface of the coupons was determined, cross-sectional slices in the streamwise direction of the channel were analyzed to calculate the cross-sectional area and the perimeter of each slice. These were then used to calculate D_h of the internal channel as a function of streamwise distance. The average D_h of the internal channel in the region downstream of the film cooling holes is reported in Table 1 as $D_{h,i}$.

The same approach of examining cross-sectional slices was used to calculate the cross-sectional area, A_c, of the film cooling holes. Here, however, the slices were taken along the hole axis. A_c (normalized by the specified meter area $\pi D^2/4$) was then calculated for each slice as a function of distance along the hole axis, ℓ, and is shown in Fig. 4. A solid black line indicates the nominal A_c according to the part specification. The darker dotted lines represent the mean A_c for all holes in a given coupon. The light dotted lines on the chart represent the A_c of all the holes; these are included to show the hole-to-hole variation of a given coupon.

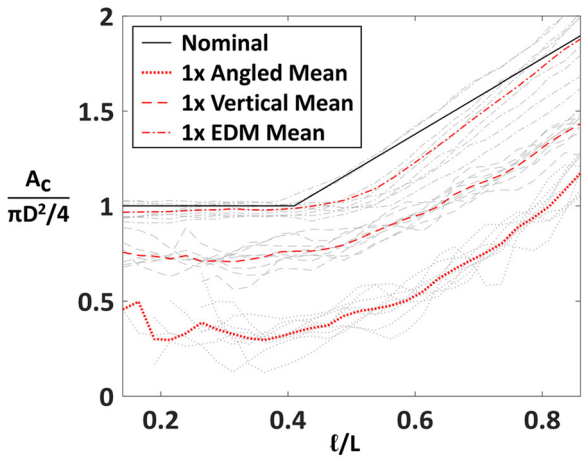

Fig. 4 Cross-sectional area of film holes as a function as axial distance along the film hole in the direction of flow

One can quickly glean from Fig. 4 that on average, both build directions of AM holes at 1× scale are smaller than the specified value with the angled build direction resulting in a A_c that is approximately half that of the nominal A_c. One will also note that the angled coupon has a larger hole-to-hole variation than the vertical coupon with some of the holes being almost completely closed off somewhere in the metering section.

Qualitative results of the data presented in Fig. 4 are shown in Fig. 5. This figure shows cross section of the CT reconstruction of one film hole from each of the six coupons with film holes. The black regions represent the solid material and the white regions represent the hole. Large roughness features blocking the flow are easily visible in the 1x-A-1H-AM and the 1x-A-2H-AM coupons as seen in Figs. 5(*a*) and 5(*d*), respectively. The EDM hole shown in Fig. 5(*c*) appears smooth considering the resolution of the CT scanner. Roughness is observed in the 2× film holes (Figs. 5(*e*) and 5(*f*)), but the roughness is not as prominent due to the larger hole diameter. The roughness on the 2x-V-1H-AM coupon has only slightly altered the shape of the hole from the intended design.

Micrographs of the film cooling holes were collected with a scanning electron microscope. Figure 6 shows images of holes from three different coupons (1x-V-1H-AM, 1x-A-2H-EDM, 2x-A-1H-AM) each from two different perspectives. The regions of very dark gray and black in Figs. 6(*d*) and 6(*e*) are the black paint that was not completely removed before imaging. The top three images (Figs. 6(*a*)–6(*c*)) were collected with the view aligned with the axis of the hole, Fig. 6(*a*) shows blockage on the top region of the hole at the exit in the 1x-V-1H-AM coupon. This blockage is a burr resulting from the grinding process used to smooth the external surface. One can also see that the roughness in the metering section protrudes from the walls well into the flow path.

The holes drilled with EDM have a much smaller roughness, which renders the hole nearly circular in the metering section (Fig. 6(*b*)). The metering section of the 2x-A-1H-AM holes (Fig. 6(*c*)) appears to be shaped more like an angled ellipse than a circle. This is due to the angled build direction. The upper left region of this hole was an unsupported surface that somewhat collapsed during the build and effectively added blockage to the hole. This result is not surprising for holes built at such angles. For the 1x-A-1H-AM coupon, this phenomenon is responsible for the blockage seen in Fig. 5(*a*). However, the larger hole size of the 2x-A-1H-AM coupon reduces how detrimental this effect can be on flow through the hole.

Also seen from the scanning electron microscope micrographs is the relative roughness between each hole size and manufacturing method. Figures 6(*d*)–6(*f*) show that the roughness in the 1× holes are larger relative to the hole diameter than the 2×. With regard to the AM roughness observed here, the EDM hole appears to be very smooth although there is some roughness present.

As with flow through any orifice, the fluid flow rate through the film cooling holes scales with the minimum area. Therefore, the minimum area was used in the calculation of M of the film cooling holes. The minimum area of each hole was obtained from the CT scan analysis. Because there is hole-to-hole variation in minimum cross-sectional area (as exhibited in Fig. 4), an average minimum cross-sectional area was calculated by averaging the minimum areas of all the film holes. This average minimum cross section area is given in Table 1 as $A_{min,avg}$.

The final necessary geometric scale for these experiments was the coupon wall thickness, t, separating the coolant flow from the external flow over the coupon. Spatially resolved thickness was calculated using tools in the reconstruction and analysis software package. The standard deviation of wall thickness for all coupons was between 0.06 and 0.11 mm. Average values of t are reported in Table 1.

Results

The flow and heat transfer results of this study are presented in five different parts. First, the effects of internal roughness and

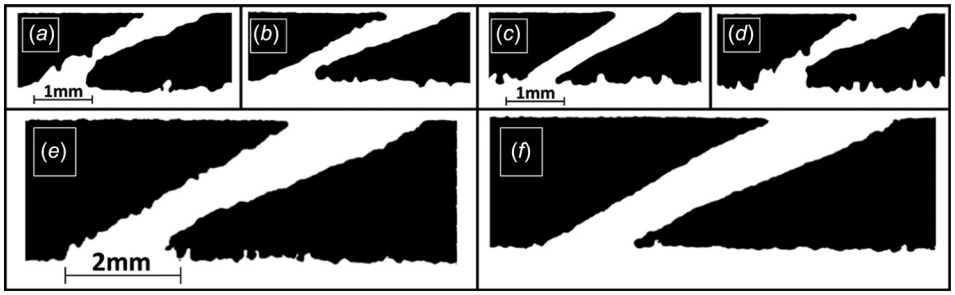

Fig. 5 Cross section of coupon at one film hole obtained from CT scan on the (*a*) 1x-A-1H-AM, (*b*) 1x-V-1H-AM, (*c*) 1x-A-2H-EDM, (*d*) 1x-A-2H-AM, (*e*) 2x-A-1H-AM, and (*f*) 2x-V-1H-AM coupons showing the as built shape

height of the coolant channel on the effectiveness will be discussed. The data presented in this section came from coupons without film cooling holes. This is followed by results of pressure drop and flow rate measurements made of flow through the film cooling holes. Next, film cooling results are presented, beginning with a section that discusses a comparison of the two hole manufacturing methods. In the Internal Geometry Effects section, the effect of M on ϕ for the $1\times$ and $2\times$ scale coupons is described. Finally, the impact of the build direction on ϕ is presented.

Internal Geometry Effects. To evaluate the contribution to overall effectiveness of convection in the coolant channel, the baseline coupons (1x-A-2H-BL, 1x-V-1H-BL, 2x-A-1H-BL, 2x-V-1H-BL) were tested over a range of internal Reynolds numbers all at a fixed Bi. The area-averaged effectiveness, $\bar{\bar{\phi}}$ is given as a function of the heat load parameter, HLP, in Fig. 7. $\bar{\bar{\phi}}$ was calculated by averaging ϕ from the trailing edge of the film hole to $x/D = 20$ in the streamwise direction and $S/D = 18$ in the lateral direction. Also shown in Fig. 7 are lines of constant internal effectiveness, η_{th}, calculated using Eq. (3) from Ref. [24]. These lines were manually fit to the experimental data to determine η_{th} of each of the coolant channels. Figure 7(*a*) shows the effectiveness of the $1\times$ coupons. Of these two baseline coupons, the one with the smaller internal channel (1x-V-1H-BL) has a higher overall effectiveness for a given HLP than the coupon with the larger channel (1x-A-2H-BL). This is the result of two combined effects

$$\phi = \frac{\eta_{\text{th}}\text{HLP}}{1 + \eta_{\text{th}}\text{HLP}} \tag{3}$$

The first is the effect of Re_i. Because HLP is not scaled by internal geometry, keeping HLP constant results in a higher Re_i for the 1x-V-1H-BL. This naturally increases the internal convection and therefore the overall effectiveness. Relative roughness, $R_a/D_{h,i}$, is the other contributing effect to the difference in

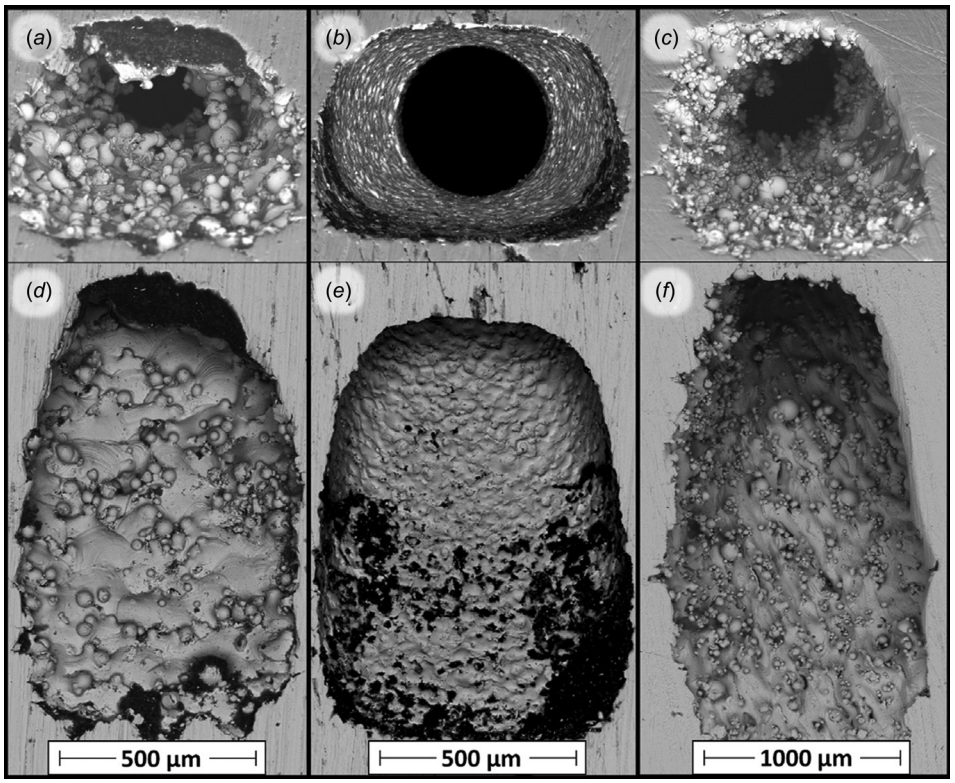

Fig. 6 Scanning electron microscope micrographs of film cooling holes with the view aligned to the film hole axis for the (*a*) 1x-V-1H-AM, (*b*) 1x-A-2H-EDM, and (*c*) 2x-A-1H-AM coupons, and with the view aligned normal to the coupon top surface for the (*d*) 1x-V-1H-AM, (*e*) 1x-A-2H-EDM, and (*f*) 2x-A-1H-AM coupons

effectiveness. Previous measurements showed that the absolute roughness is comparable between the coupons [3]. However, $D_{h,i}$ of the 1x-A-2H-BL coupon is twice as large implying that $R_a/D_{h,i}$ is smaller. Therefore, the effectiveness of the 1x-V-1H-BL coupon is also further augmented due to relative roughness.

Figure 7(*b*) shows the data for the 2x-A-1H-BL and 2x-V-1H-BL coupons. Because these coupons have a comparable internal channel roughness and similar $D_{h,i}$, they give the same effectiveness for a given HLP. One will note that the effectiveness is lower for the 2× coupons than the 1× coupons, even though the 1x-A-2H-BL has a comparable $D_{h,i}$. The reason for this is that Bi was fixed for each test by adjusting h_∞. Because the 2× coupons have a thicker wall, h_∞ must be lower to match Bi. This gives a smaller h_∞/h_i for the 2× coupons.

An analysis was carried out to determine the thermal effectiveness of theoretical smooth channels with dimensions matching the AM channels' measured dimensions. The internal heat transfer coefficient, h_i, was predicted using a smooth channel correlation based on Re along with Eq. (4) to calculate internal effectiveness. These values are given as dashed lines in Fig. 7. Comparing these smooth calculations to the fit line of the experimental results, one can see the significant increase in internal effectiveness of the 1× AM channels (Fig. 7(*a*)) simply due to the increased roughness. The AM roughness resulted in an increase in effectiveness of approximately 0.15 relative to the theoretical smooth coupon for HLP > 1. The increase in effectiveness for the 2× AM channels (Fig. 7(*b*)) was smaller, which is primarily due to the fact that the 2× channels have a larger HLP for a given flow rate, due to the increased h_∞ mentioned earlier.

$$\eta_{\text{th}} = 1 - \exp\left[\frac{-1}{\dot{m}_c c_{p,c}\left(\frac{1}{A_s h_i} + \frac{t}{A_s \kappa}\right)}\right] \tag{4}$$

Flow Results. Prior to the heat transfer tests with the film cooling coupons, flow tests were conducted as previously described.

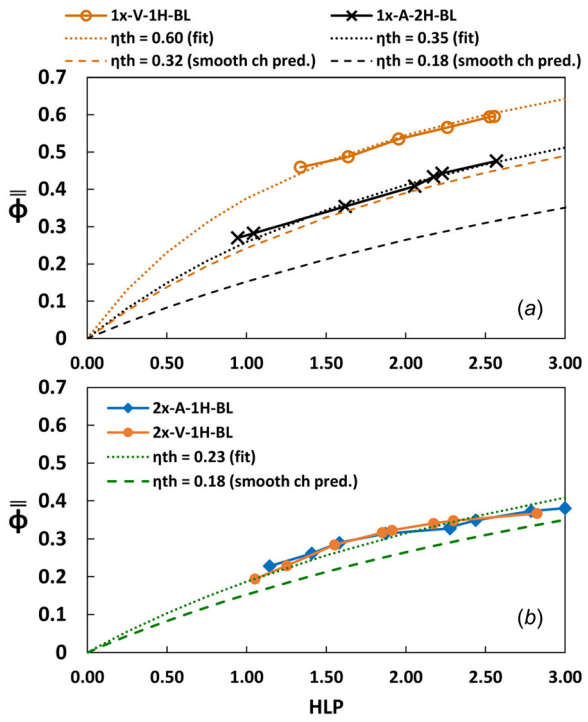

Fig. 7 Area-averaged effectiveness versus HLP for (*a*) 1× baseline coupons and (*b*) 2× baseline coupons. Dotted and dashed lines of constant internal effectiveness.

Results from these tests are shown in Fig. 8 as FP versus PR. Figure 8 clearly shows that each coupon had its own characteristic flow curve. The film holes with the lowest FP for a given PR were the 1x-A-2H-AM and the 1x-A-1H-AM. These AM coupons are also the two that had the roughest and most blocked film holes as observed in Fig. 5. The film holes with the highest flow parameter were the EDM holes. The EDM holes were observed to be the smoothest of all the holes shown in Fig. 5. The film holes with the next highest FP are the 2x-V-1H-AM, which appear in Fig. 5 to be the next smoothest after the EDM hole. The remaining two film holes follow the same trend of the roughness being inversely proportional to FP. The difference between the lowest flow parameter curve and the highest is almost a factor of three. These results show the significant role that roughness plays in limiting the flow through a film cooling hole for a fixed PR.

Manufacturing Method Effects: EDM Versus AM. Cooling effectiveness of the coupon with the EDM film cooling holes was compared to the effectiveness of the coupons with holes made with AM. Recall that for every coupon, the internal supply channels were rough since they were all made using AM. Contour plots of the overall effectiveness for the 1x-2H-A-EDM and the 1x-2H-A-AM coupons are given in Fig. 9 for two different Re_i at $M = 1.2$. For the EDM holes, peaks in effectiveness downstream of each hole indicated the presence of film cooling as far as 20*D* in the streamwise direction. Additionally, these peaks in effectiveness were of similar magnitude for each of the three holes, showing relatively consistent film cooling coverage.

The area-averaged effectiveness, $\bar{\phi}$, is shown in Fig. 10 for these two coupons. Maintaining a constant Re_i ensured that the contribution to effectiveness from the internal cooling was identical for both coupons. Over the range of blowing ratios shown, the EDM holes showed a higher overall effectiveness than the AM holes for a given Re_i. Increasing Re_i increased h_i, which resulted in a higher effectiveness regardless of the manufacturing technique of the film holes or to blowing ratio. Increasing the blowing ratio also caused an increase in effectiveness for both types of holes.

While the presence of film cooling was also evident downstream of the AM holes, the peaks in effectiveness were lower than the peaks from the EDM holes. This decrease in film effectiveness can be attributed to two different phenomena. First, the mass flow rate through the AM holes is much lower than the flow rate through the EDM holes at a given *M*. This is due to the decreased metering area in the AM holes which was used to scale *M*. A lower flow rate of coolant ultimately leads to a lower film effectiveness. The second phenomenon has to do with the flow physics of coolant exiting a rough hole. As was first shown by Schroeder and Thole [15] using thermal and flowfield measurements, increased in-hole surface roughness of shaped film cooling holes results in a coolant jet extending higher above the wall and

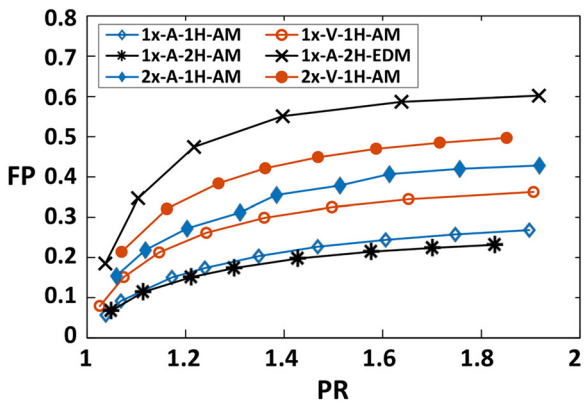

Fig. 8 Flow parameter versus PR for all film holes

spreading less laterally than a smooth hole. These differences are a result of the roughness features generating a thicker boundary layer in the hole, resulting in a jet core with a higher velocity. In addition to creating a coolant jet with higher momentum, the presence of roughness in the hole generates higher turbulence in the jet. The combination of these two effects leads to an ineffective film cooling jet that is prone to liftoff and increased mixing with the mainstream. In the current study, the roughness from the AM process generated these unfavorable coolant jet characteristics, decreasing the effectiveness of the film holes relative to holes made with EDM.

Not only did the AM holes fail to cool the surface as effectively as the EDM holes, but they also showed inconsistent cooling between different holes in a given coupon as seen in Fig. 9. The hole located at $S/D = 6$ had the highest effectiveness peak, followed by the hole at $S/D = -6$, while the center hole showed no peak in downstream effectiveness. Furthermore, the cooling around the holes to due to in-hole convection followed the same trend, indicating more coolant was ejected from the hole at $S/D = 6$. Due to random nature of AM roughness and the small scale of the 1× film holes in this study, identical holes in a given coupon were subject to varying levels of roughness and blockage. This phenomenon was illustrated in Fig. 4, where there was a large variation in the measured cross-sectional areas of the holes.

Scale Effects: 1× Versus 2×. Effectiveness data from the 1× coupons are shown alongside data from the 2× coupons in Fig. 11. The horizontal lines in Figs. 11(*a*) and 11(*b*) represent the area-averaged effectiveness for coupons without film cooling holes that have the same internal channel dimensions as the 1× and 2× coupons. Figure 11(*a*) shows area-averaged effectiveness versus blowing ratio at $\mathrm{Re}_i = 14{,}000$. Two major trends were observed in these data. First, there was a noticeable difference in the magnitude of effectiveness between the 1× AM and the 2× AM coupons. Since the absolute roughness of the AM process is presumed to be constant for a given build direction, the relative roughness, $R_a/D_{h,i}$, of the internal channel of the 1× coupon is greater than that of the 2× coupon because $D_{h,i}$ is greater. As was shown in the authors' previous work [4], the internal heat transfer coefficient of AM channels scales with relative roughness.

The second trend illustrated in Fig. 11(*a*) is the difference in sensitivity of area-averaged effectiveness to blowing ratio. The 1× coupons showed an increase in area-averaged effectiveness with increased M while the 2× coupons did not respond to changes in M for $M < 3$. The area-averaged effectiveness results for the 1x-A-2H-EDM coupon are also shown on Fig. 11(*a*) for comparison. The trend of the EDM hole is consistent with the performance of shaped film cooling holes with the maximum effectiveness observed around $M = 2$ [19].

Because the contribution of internal cooling to overall effectiveness was constant at all blowing ratios for a given internal channel size, the explanation for the difference in effectiveness trends between the 1× and the 2× coupons lies in the varying film effectiveness and in-hole convection of each coupon. Schroeder and Thole [15] studied film effectiveness for the same hole geometry chosen in this study at comparable values of in-hole relative roughness. Schroeder's results showed a monotonic decrease in area-averaged film effectiveness with increased M. The reason for this was described previously in the discussion on the decrease in effectiveness of the AM holes compared to the EDM holes.

In-hole convection has been shown in literature to contribute to a significant portion of the cooling effectiveness [25,26]. As much as 30–50% of the total heat absorbed by the cooling flow has been attributed to the flow passing through the holes in different types of film cooling configurations. Since the film holes in this study were rougher than traditional holes, an augmentation of in-hole convection was expected. In an attempt to quantify the effect of in-hole convection, overall cooling effectiveness was averaged in the regions beside the holes extending to $\pm 9D$ in the lateral direction and from the leading to trailing edge of the holes in the streamwise direction. Data in the footprint of the hole were excluded from this average. These regions were not exposed to any film cooling; therefore, the effectiveness measured in these regions was due to convection within the film hole and coolant channel only. By holding Re_i constant, convection in the coolant channel was also held constant, and the changes in effectiveness near the holes were attributed to the in-hole convection only. This area-averaged effectiveness for the near-hole region, $\bar{\bar{\phi}}_h$, is shown versus blowing ratio in Fig. 12. As expected, an increase in coolant flow through the hole resulted in stronger in-hole convection. This trend is monotonic as could be predicted.

Since film effectiveness and the in-hole convection have opposite trends with increasing blowing ratio, the fact that the overall effectiveness was stagnant for $M < 3$, was hypothesized to be the result of these two contributions offsetting each other. The decrease in film effectiveness coincidentally matched the increase of in-hole convection with blowing ratio for these particular 2× coupons. This hypothesis is supported by the data plotted in Fig. 13, which shows the average centerline effectiveness, ϕ_{CL}. This value was calculated by taking the centerline effectiveness of the middle three holes and averaging those results. For both 2× coupons, a larger peak in effectiveness was observed immediately downstream of the hole for $M = 3$, but this peak decayed faster with X/D than the $M = 1.2$ data. This indicates stronger in-hole convection at higher blowing ratios since film effectiveness is expected to be lower just downstream of the laid back diffused hole at higher blowing ratio [19].

For $M > 3$, the effect of in-hole convection reached farther downstream, while the decrease in film effectiveness leveled off,

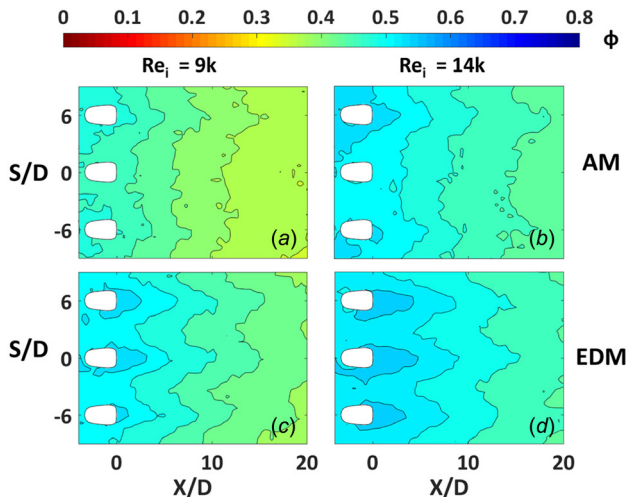

Fig. 9 Contours of area-averaged effectiveness at $M = 1.2$ for AM holes ((*a*) and (*b*)) and EDM holes ((*c*) and (*d*))

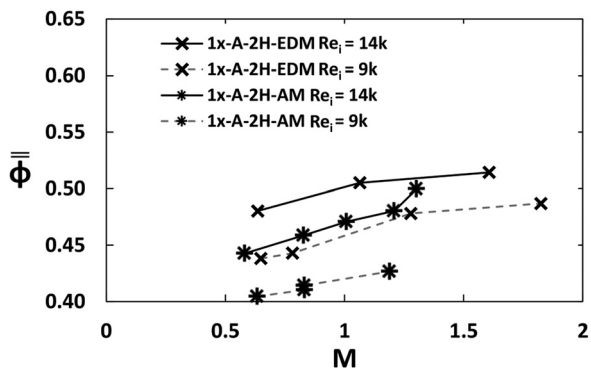

Fig. 10 Area-averaged effectiveness of 1× AM and EDM

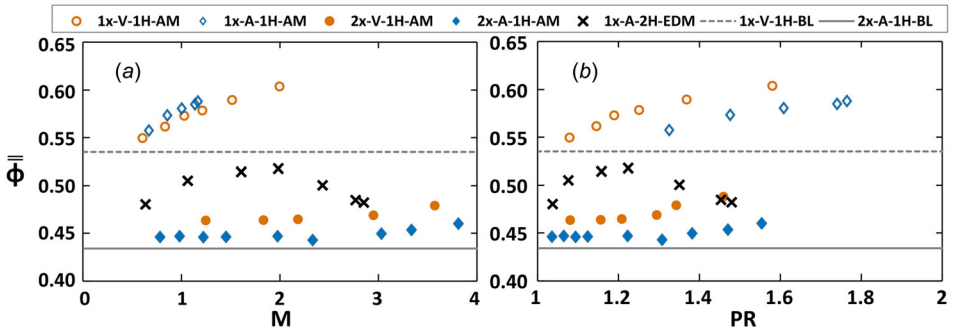

Fig. 11 Area-averaged effectiveness versus (*a*) blowing ratio and (*b*) PR at $Re_i = 14{,}000$

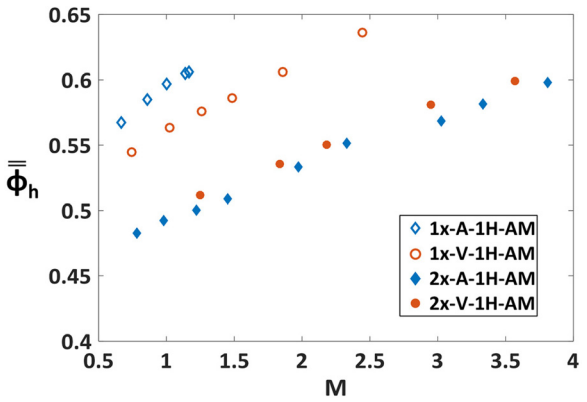

Fig. 12 Area-averaged effectiveness from leading to trailing edge of the hole, $\pm 9D$ in lateral direction at $Re_i = 14{,}000$

resulting in the upward trend of the overall effectiveness curve at the highest blowing ratios. Since the 1× holes had a higher relative roughness than the 2× holes, the heat transfer augmentation inside the hole was larger, while the film effectiveness was lower. Therefore, the in-hole convection was the dominant heat transfer mechanism in the 1× coupons, causing the increase in overall effectiveness seen in Fig. 11(*a*).

Because pressure ratio is a useful parameter for gas turbine engine design, the effectiveness data plotted in Fig. 11(*a*) were also plotted against PR and is shown in Fig. 11(*b*). In conventional gas turbine engines, the components exposed to the highest heat loads are often those that have the lowest available coolant PR. In practice, these highest heat load components will probably operate in the left most region of Fig. 11(*b*) because of the low available PR. This suggests that film effectiveness will not contribute significantly to the overall cooling of these components. This is particularly true for the 1× coupons built in the angled direction because of their low flow rates for all pressure ratios. However, benefits can still be found due to augmented in-hole convection for all *M* or PR.

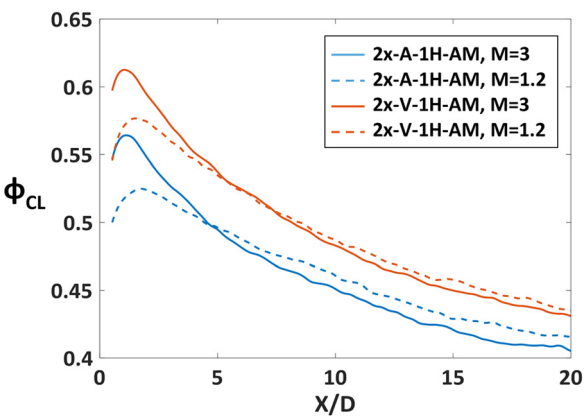

Fig. 13 Average centerline effectiveness of three holes for two different blowing ratios at $Re_i = 14{,}000$

Build Direction Effects. The overall cooling effectiveness of different build directions for the 2× coupons is compared in contour plots shown in Fig. 14 at two different blowing ratios. At both low and high blowing ratios, the vertically built holes provided better film cooling coverage than the holes built at an angle as seen by the peaks in the contours. At the low blowing ratio, the presence of film cooling was seen for both build directions, with the vertical build direction having higher effectiveness. However, at the high blowing ratio, there was little evidence of film cooling in the angled build direction case, indicating film cooling jet liftoff. This result can be explained by the higher surface roughness in the holes built angled than the holes built vertically, as shown in Figs. 4(*e*) and 4(*f*), respectively. This roughness trend is consistent with the authors' previous study of build direction effects on the roughness of cylindrical holes [1]. As mentioned earlier, the larger surface roughness results in greater jet momentum for shaped film cooling holes, causing the jet to liftoff, decreasing film effectiveness.

Conclusions

As the use of additive manufacturing increases among gas turbine manufacturers, it is important to understand how the additive manufacturing process affects the thermal performance of airfoil

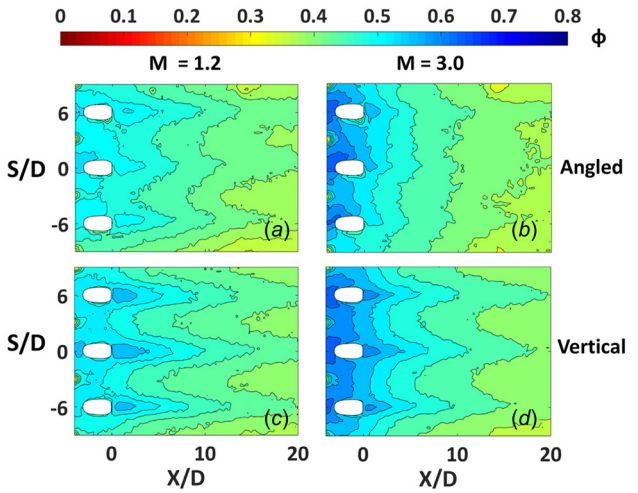

Fig. 14 Contours of area-averaged effectiveness at $Re_i = 14{,}000$ for 2× holes at angled build direction ((*a*) and (*b*)) and vertical build direction ((*c*) and (*d*))

cooling configurations. For this reason, test coupons with engine scale shaped film cooling holes were manufactured out of a high-temperature nickel alloy using laser powder bed fusion. These coupons were tested at engine representative conditions to evaluate the effects of geometric parameters and flow conditions on overall cooling effectiveness.

Characterization of the geometry with X-ray computed tomography and scanning electron microscopy showed the significant impact additive manufacturing had on the hole shape. Coupons with the smaller sized holes built at an angle relative to the build direction had holes that were almost completely blocked off. However, the coupons with holes built at a favorable build orientation were less blocked, allowing for more flow. Similarly, the larger size holes showed greater blockage for the angled build orientation than the vertical orientation, but the blockage on these larger holes built at an angle did not decrease the flow in the same proportion as the blockage in the smaller holes built at an angle. Attempting to manufacture small holes in a turbine component without an iterative design process will result in undersized or even blocked holes. Building larger holes with additive manufacturing will give a much better chance of producing a hole that is close to the specification, while decreasing the relative roughness in the hole.

Heat transfer experiments showed that the roughness of the additive manufacturing process significantly influenced the overall effectiveness through several mechanisms: film cooling, in-hole convection, and internal convection. The significant blockage in the smaller holes minimized mass flow of coolant through the hole for a given pressure ratio which limited the contribution of film cooling to the overall effectiveness. On the other hand, the relatively smooth EDM holes had a higher overall effectiveness than the AM holes due to increased film effectiveness. The effectiveness of the coupons with the larger holes showed a greater dependence on build direction and roughness than did the coupons with smaller holes. Of the coupons with larger holes, those built vertically showed better film performance than those built at an angle. All holes tested showed signs of significant in-hole convection due to the in-hole roughness. However, the internal cooling was observed to have the greatest impact on the overall thermal performance due to the significant augmentation of the internal convection resulting from the internal channel roughness.

From the results of this study, it is evident that there are many effects of the AM process on overall cooling performance of film cooling holes. Applying additive manufacturing to the production of film cooled turbine parts requires strategies such as scaling the hole dimensions, specifying alternative cross section area geometries in the metering section, and controlling hole orientation relative to the build direction in order to produce holes with predictable geometries, surface roughness, and cooling performance. This study provides a base of knowledge for designers to understand the implications of manufacturing film cooling designs using AM.

Acknowledgment

The authors would like to thank Pratt & Whitney for the financial and technical assistance throughout this study. They would also like to express thanks to Corey Dickman and Griffin Jones at CIMP-3D for assisting in the building and CT scanning of the test specimen that made this work possible.

Nomenclature

A_c = cross-sectional flow area
$A_{\min}$ = minimum cross-sectional area of cooling hole meter
A_s = surface area
Bi = Biot number, $h_\infty t/\kappa$
c_p = specific heat capacity
D = film hole metering section diameter
D_h = hydraulic diameter, $4A_c/p$
DR = density ratio, ρ_c/ρ_∞
FP = mass flow parameter, $\dot{m}\ (\mathrm{RT}_c)^{0.5}/P_cA_c$
h = convective heat transfer coefficient
H = mainstream channel height
HLP = heat load parameter, $\dot{m}_c^p{}_{,c}/(A_sh_\infty)$
ℓ = length coordinate along axis of film cooling hole
L = hole length
$\dot{m}$ = mass flow rate
M = blowing ratio, $(\dot{m}_f/A_{\min})/(\rho_\infty U_\infty)$
Ma = Mach number
Nu = Nusselt number, hD_h/κ_{air}
p = wetted perimeter
P = pressure
Pr = Prandtl number
PR = pressure ratio
R = gas constant
R_q = arithmetic mean roughness
Re = Reynolds number, VD_h/ν
S = lateral distance between holes, pitch
t = coupon wall thickness
T = temperature
U = maximum/centerline velocity
V = mass average velocity
x = streamwise distance

Greek Symbols

η_{th} = internal effectiveness
κ = thermal conductivity of coupon
κ_{air} = thermal conductivity of air
ν = kinematic viscosity
ρ = fluid
ϕ = overall effectiveness, $(T_\infty - T_s)/(T_\infty - T_c)$
$\bar{\phi}$ = area-averaged overall effectiveness

Subscripts

avg = averaged
c = coolant
cl = centerline of film hole
f = film cooling flow
h = region on surface adjacent to film hole breakout
i = coupon internal channel
s = coupon surface
∞ = mainstream

References

[1] Snyder, J. C., Stimpson, C. K., Thole, K. A., and Mongillo, D., 2015, "Build Direction Effects on Microchannel Tolerance and Surface Roughness," ASME J. Mech. Des., **137**(11), p. 111411.
[2] Snyder, J. C., Stimpson, C. K., Thole, K. A., and Mongillo, D., 2016, "Build Direction Effects on Additively Manufactured Channels," ASME J. Turbomach., **138**(5), p. 051006.
[3] Stimpson, C. K., Snyder, J. C., Thole, K. A., and Mongillo, D., 2016, "Roughness Effects on Flow and Heat Transfer for Additively Manufactured Channels," ASME J. Turbomach., **138**(5), p. 051008.
[4] Stimpson, C. K., Snyder, J. C., Thole, K. A., and Mongillo, D. J., 2017, "Scaling Roughness Effects on Pressure Loss and Heat Transfer of Additively Manufactured Channels," ASME J. Turbomach., **139**(2), p. 021003.
[5] Hanson, R. B., 2014, "Combustor Component With Cooling Holes Formed by Additive Manufacturing," United Technologies Corporation, Farmington, CT, U.S. Patent No. 20140216042 A1.
[6] Xu, J., 2014, "Gas Turbine Engine Shaped Film Cooling Hole," United Technologies Corporation, Farmington, CT, U.S. Patent No. 20160003056 A1.
[7] Johnson, T. E., Keener, C. P., Ostebee, H. M., and Wegerif, D. G., 2016, "Effusion Plate Using Additive Manufacturing Methods," General Electric Company, Boston, MA, U.S. Patent No. 20140202163 A1.
[8] Dudebout, R., Brandt, D., Waldman, D., Neumann, J., and Payne, A., 2016, "Gas Turbine Engine Combustors With Effusion and Impingement Cooling and Methods for Manufacturing the Same Using Additive Manufacturing Techniques," Honeywell International Inc., Morris Plains, NJ, U.S. Patent No. 20150226433 A1.
[9] Schurb, J., Hoebel, M., Haehnle, H., Kissel, H., Bogdanic, L., and Etter, T., 2016, "Additive Manufacturing of Hot Gas Path Parts and Engine Validation in a Heavy Duty GT," ASME Paper No. GT2016-57262.
[10] Vinton, K. R., Nahang-Toudeshki, S., Wright, L. M., and Carter, A., 2016, "Full Coverage Film Cooling Performance for Combustor Cooling Manufactured Using DMLS," ASME Paper No. GT2016-56504.

[11] Jackowski, T., Schulz, A., Bauer, H.-J., Gerendás, M., and Behrendt, T., 2016, "Effusion Cooled Combustor Liner Tiles With Modern Cooling Concepts: A Comparative Experimental Study," ASME Paper No. GT2016-56598.
[12] Aghasi, P., Gutmark, E., and Munday, D., 2016, "Dependence of Film Cooling Effectiveness on 3D Printed Cooling Holes," ASME Paper No. GT2016-56698.
[13] Kirollos, B., and Povey, T., 2017, "Laboratory Infra-Red Thermal Assessment of Laser-Sintered High-Pressure Nozzle Guide Vanes to De-Risk Engine Design Programmes," ASME J. Turbomach., **139**(4), p. 041009.
[14] Krawciw, J., Martin, D., and Denman, P., 2015, "Measurement and Prediction of Adiabatic Film Effectiveness of Combustor Representative Effusion Arrays," ASME Paper No. GT2015-43210.
[15] Schroeder, R. P., and Thole, K. A., 2017, "Effect of In-Hole Roughness on Film Cooling From a Shaped Hole," ASME J. Turbomach., **139**(3), p. 031004.
[16] Schroeder, R. P., 2015, "Influence of In-Hole Roughness and High Freestream Turbulence on Film Cooling From a Shaped Hole," Ph.D. dissertation, Pennsylvania State University, State College, PA.
[17] Albert, J. E., Bogard, D. G., and Cunha, F., 2004, "Adiabatic and Overall Effectiveness for a Film Cooled Blade," ASME Paper No. GT2004-53998.
[18] Bunker, R. S., 2009, "The Effects of Manufacturing Tolerances on Gas Turbine Cooling," ASME J. Turbomach., **131**(4), p. 041018.
[19] Schroeder, R. P., and Thole, K. A., 2014, "Adiabatic Effectiveness Measurements for a Baseline Shaped Film Cooling Hole," ASME Paper No. GT2014-25992.
[20] EOS GmbH, 2014, "Material Data Sheet: EOS NickelAlloy HX," EOS GmbH, Munich, Germany.
[21] EOS GmbH, 2011, "*Basic Training EOSINT M 280*," EOS GmbH, Munich, Germany.
[22] Kays, W. M., Crawford, M. E., and Weigand, B., 2004, *Convective Heat & Mass Transfer*, McGraw-Hill, Boston, MA.
[23] Reinhart, C., 2011, *Industrial CT & Precision*, Volume Graphics GmbH, Heidelberg, Germany.
[24] Downs, J. P., and Landis, K. K., 2009, "Turbine Cooling Systems Design: Past, Present and Future," ASME Paper No. GT2009-59991.
[25] Martiny, M., Schulz, A., and Wittig, S., 1997, "Mathematical Model Describing the Coupled Heat Transfer in Effusion Cooled Combustor Walls," ASME Paper No. 97-GT-329.
[26] Falcoz, C., Weigand, B., and Ott, P., 2006, "A Comparative Study on Showerhead Cooling Performance," Int. J. Heat Mass Transfer, **49**(7–8), pp. 1274–1286.